Available online at www.sciencedirect.com

ScienceDirect

Ceramics International 40 (2014) 2337–2342

CERAMICS INTERNATIONAL

www.elsevier.com/locate/ceramint

A novel TiO_2 nanorod/nanoparticle composite architecture to improve the performance of dye-sensitized solar cells

Min Zhu*, Ling Chen, Haibo Gong, Min Zi, Bingqiang Cao*

Key Laboratory of Inorganic Functional Materials in Universities of Shandong, School of Materials Science and Engineering, University of Jinan, Jinan 250022, China

Received 26 July 2013; received in revised form 1 August 2013; accepted 1 August 2013
Available online 9 August 2013

Abstract

In this article, we first prove that the length increase of TiO_2 nanorods by extending reaction time is infeasible for improving dye-sensitized solar cells (DSSCs) efficiency because the longer growth time will lead to combination of nanorods from the roots part and formation of dense film. Then a TiO_2 nanorod-nanoparticle mesoporous film composite anode structure is designed and fabricated that serves as a model architecture for efficient cell devices as it simultaneously offers a large surface area, good light-scattering characteristics and a highly conductive pathway for charge carrier collection. Under standard solar cell measurement conditions, a photovoltaic conversion efficiency of 2.51% is obtained from the nanorod-nanoparticle film composite structure, which is higher than that of pure TiO_2 nanorods DSSC (1.11%). By another surface treatment process with $TiCl_4$, the DSSC efficiency based on such composite TiO_2 anode is further improved to 3.25%.

Keywords: TiO_2 nanorods; Dye-sensitized solar cells; Composite anode; Surface treatment

1. Introduction

In the past few decades, dye-sensitized solar cells (DSSCs) have been extensively investigated as a promising alternative to conventional solar cells based on p–n junction due to its low-cost manufacture [1,2]. A traditional DSSC is composed of organic dye, iodide electrolyte, Pt counter-electrode and photoanode which are all the key components for the photovoltaic conversation. Many research groups have tried to improve the DSSCs power conversion efficiency by controlling the structure of anode [3,4]. The usual porous nanocrystalline TiO_2 film offers a big surface area to absorb enough dye. However, the porous structure is not in favor of electron transport due to the multiple transport paths among different grain boundaries [5–7]. Therefore, one-dimensional nanostructure such as nanorod [8–10] or nanotube [11–13] arrays have been adopted to address this issue. They offer direct electrical pathways for electron due to the single crystal structure. But the conversion efficiency is still low because of smaller photoanode surface area caused by limited nanowire/nanotube length. Additionally, the growth of longer TiO_2 nanorods is also difficult due to combination of nanorods from root parts [14]. Therefore, some researchers developed composite semiconductor films to enhance the light harvesting efficiency and electron transport [15,16]. For example, Sheng et al. [15] added TiO_2 nanotubes (5% content) into porous nanoparticle film and obtained a high power conversion efficiency of 9.79%, as single-crystal nanotube has a longer electron lifetime and less combination loss occurs at the interface. Peng et al. [16] showed that the efficiency of a composite DSSC was improved after 24 wt% rutile nanorods were added to mesoporous film. However, these TiO_2 nanorods are randomly mixed into nanoparticles with inferior electron transport property compared to vertically aligned nanorod or nanotube arrays on the conductive substrate. Therefore, how to efficiently increase the anode specific surface area, transfer electrons and reduce their recombination with redox species is believed to be the key steps in achieving more efficient DSSCs.

In this paper, we design and prepare a new kind of composite anode structure that a layer of TiO_2 nanoparticle

---

*Corresponding authors. Tel.: +86 531 89736292; fax: +86 531 87974453.
E-mail address: mse_caobq@ujn.edu.cn (B. Cao).

0272-8842/$ - see front matter
http://dx.doi.org/10.1016/j.ceramint.2013.08.003

(TiO_2 NP) film is printed onto the top of TiO_2 nanorod (TiO_2 NR_1) arrays, named TiO_2 NR_1–NP. The TiO_2 NP film composed of commercial P25 nanoparticles with large specific surface area is mesoporous, which can absorb more dye and allow electrolyte solution to penetrate through the TiO_2 NP film and into the underlying TiO_2 NR_1 arrays. For comparison, a TiO_2 nanorod (TiO_2 NR_2) arrays film of the same thickness to that of TiO_2 NR_1–NP is also synthesized by a two-step hydrothermal growth method. It is demonstrated that the cell efficiency with composite TiO_2 NR_1–NP photoanode shows two times increase than that of TiO_2 NR_2 solar cell. Moreover, after a post $TiCl_4$ immersion treating process, the cell efficiency was further increased. The reasons were investigated by quantum efficiency and electrochemical impendence spectrum measurements.

2. Experimental details

2.1. Synthesis of TiO_2 NR_1 and NR_2

TiO_2 nanorod arrays were prepared by a hydrothermal method as described by Liu and Aydil [17]. Briefly, 30 ml of deionized water was mixed with 30 ml of concentrated hydrochloric acid (37 wt%). The mixture was stirred for 5 min, and then 1.25 ml tetrabutyl titanate was added into the mixture. 15 ml of the above reaction solution was transferred to a Teflon autoclave after being stirred to be clear and preheated at 150 °C for 40 min to expel the air dissolved in the solution. Then, hydrothermal synthesis was conducted at 150 °C for 8 h. That is one growth round for TiO_2 NR_1. To obtain longer TiO_2 NR_2, the TiO_2 NR_1 obtained from the first step was used as seed and similar hydrothermal reaction was repeated. However, 30 ml of deionized water was substituted by 25 ml of deionized water and 5 ml of saturated aqueous NaCl solution. At last, the autoclave was cooled down to room temperature under flowing water. The samples were taken out and then rinsed with deionized water before drying.

2.2. Preparation of TiO_2 NR_1–NP composite film

TiO_2 paste was prepared as reported in the literature [18]. A layer of TiO_2 paste composed of commercial P25 nanoparticles was coated onto the top of TiO_2 NR_1 by a screen-printing technology and the resulting composite film was gradually heated to 450 °C for 30 min. The anodes were then immersed into 0.04 M $TiCl_4$ aqueous solution at 70 °C for 40 min followed by calcination at 450 °C for 30 min. The obtained sample was named as TiO_2 NR_1–NP–$TiCl_4$.

2.3. DSSC device fabrication

The dried TiO_2 anodes were immersed in a 0.5 mM N719 ethanol solution for 24 h to absorb dye. The dye-sensitized electrode and Pt-counter electrode were assembled together as a sandwich sealed with 25 μm thick hot-melt gasket (Surlyn 1702). The electrolyte solution composed of 0.05 M I_2, 0.5 M LiI, 0.5 M 4-tertbutylpyridine and 0.3 M DMPII in acetonitrile was injected into the device space by vacuum backfilling. The active area of final cell was 0.6×0.6 cm^2.

2.4. Anode and cell characterization

The morphology and crystal structure of anode films were examined with field emission scanning electron microscope (FE-SEM, Quanta FEG250) and X-ray diffraction (XRD, D8-Advance, Bruker), respectively. The diffused reflectance and transmittance spectra were examined by UV–vis–NIR spectrophotometer (UV-3600, Shimadzu) equipped with an integrating sphere. The current–voltage (I–V) characteristics of the DSSCs were measured with a Keithley 2612A source/meter under simulated sunlight (AM1.5, 100 mW cm^{-2}, San-Ei). The incident-photon-to-current conversion efficiency (IPCE) was measured with a QEX10 system (PV Measurement Inc.). The electrochemical impedance spectrum (EIS) was measured with a Zahner Zennium electrochemical workstation under the solar simulator illumination (100 mW cm^{-2}) at the cell open-circuit voltage. An applied perturbation voltage was 10 mV and the frequency range was from 1 MHz to 100 mHz.

3. Results and discussion

3.1. Morphology and crystal structure of different anodes

Fig. 1 shows SEM images of anode films from different angles at variable magnification. These uniform nanorods of Fig. 1(a, c) are nearly perpendicular to the FTO substrate and exhibit quadrangular prism shapes with square top facets, which is the expected TiO_2 growth habit of tetragonal crystal structure. The density of TiO_2 NR_1 is about 4×10^9 cm^{-2} and the average length is ~2 μm via a one-step hydrothermal reaction, as is shown in the inset of Fig. 1(a). By a two-step hydrothermal reaction, the length of TiO_2 NR_2 becomes twice as long and the diameter is also wider. But, the nanorods combine together at their roots and form a continuous film as shown in Fig. 1(a). The TiO_2 NR_1–NP composite film shown in Fig. 1(b) is designed to grow of nearly same thickness with the TiO_2 NR_2. The nanoparticle film printed onto the top of TiO_2 NR_1 is uniform and mesoporous as shown in both the cross-section (Fig. 1(b)) and top (Fig. 1(d)) view SEM images.

Fig. 2 shows the XRD patterns of different kinds of TiO_2 anode films. Beside the diffraction peaks from FTO substrates marked with asterisks, all other peaks in curves (a) and (c) are ascribed to tetragonal rutile phase of TiO_2 (JCPDS no. 88-1175). In comparison with the TiO_2 power diffraction pattern, the (002) peak is significantly enhanced, especially for curve (c), which indicates that longer TiO_2 nanorods grow preferentially along [001] direction as shown in SEM images. The length of TiO_2 NR_2 is extended to ~4 μm and their orientation is better with a stronger (002)-peak than that of TiO_2 NR_1. As the nanorods are not absolutely perpendicular to the substrate surface, a stronger peak of (101) crystal face is also observed. For TiO_2 NR_1–NP film shown in curve (b), additional peaks of anatase TiO_2 (JCPDS no. 21-1272) from the P25 nanoparticles also appear.

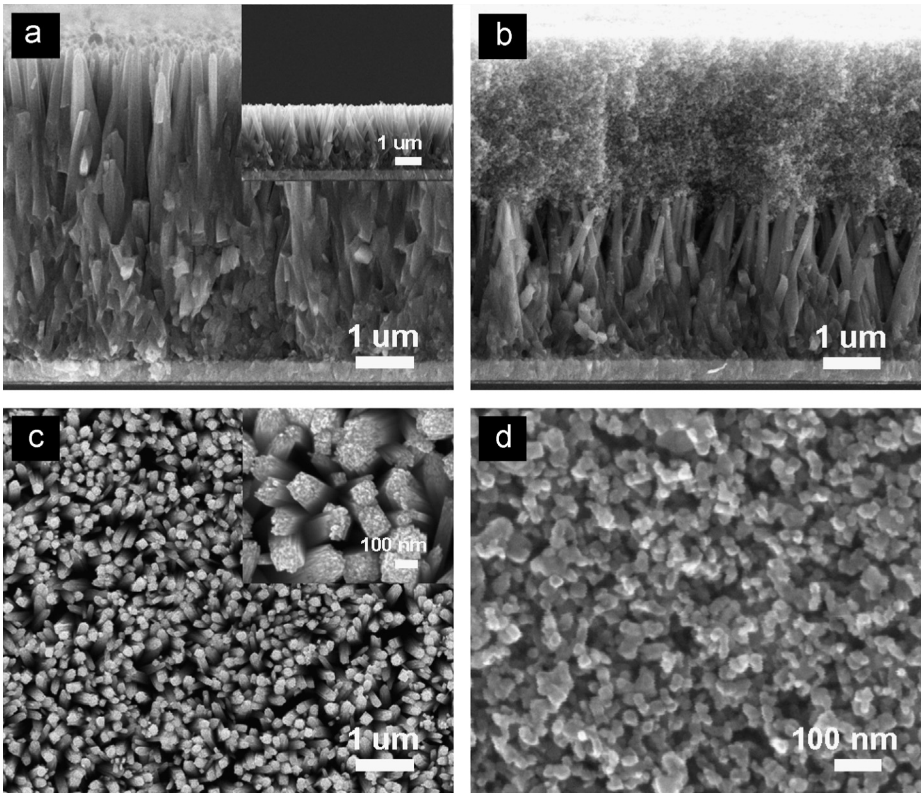

Fig. 1. Cross-sectional (a) and top view (c) SEM images of TiO_2 NR_2 film, inset of (a) is cross-sectional view of TiO_2 NR_1 film; cross-sectional (b) and top view (d) SEM images of TiO_2 NR_1–NP film.

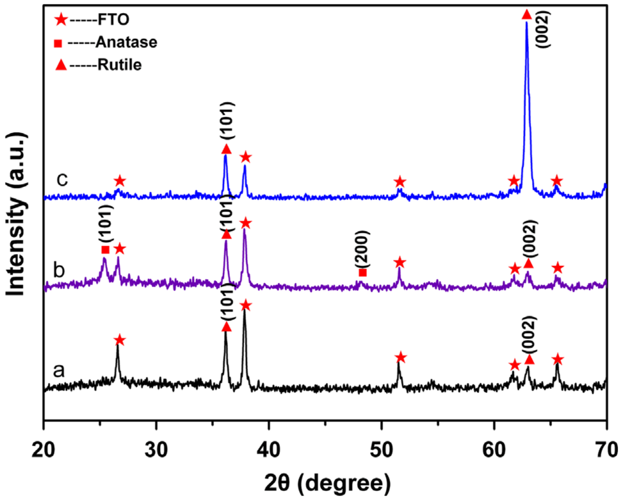

Fig. 2. XRD patterns of (a) TiO_2 NR_1, (b) TiO_2 NR_1–NP and (c) TiO_2 NR_2 films.

3.2. Optical properties and device performance

Fig. 3 shows the photocurrent–voltage (*I–V*) curves of DSSCs fabricated with different TiO_2 anodes and the according photovoltaic parameters are summarized in Table 1. The DSSC with TiO_2 NR_1 anode gets a higher short-circuit current density (J_{sc}) of 3.52 mA cm^{-2} than that (2.90 mA cm^{-2}) of TiO_2 NR_2 DSSC, which is different to our former expectation. To explore the reason, reflection and transmission properties of these two nanorod anodes were compared, as shown in Fig. 4. The reflectance of TiO_2 NR_2

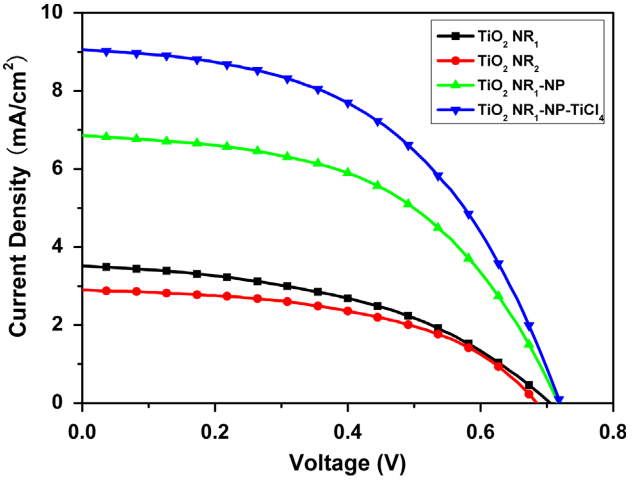

Fig. 3. *I–V* curves of the DSSCs fabricated with TiO_2 NR_1, TiO_2 NR_2, TiO_2 NR_1–NP and TiO_2 NR_1–NP–$TiCl_4$ anodes, respectively, under AM1.5 solar irradiation of 100 mW cm^{-2}.

Table 1
Photovoltaic parameters of different kinds of DSSC calculated from Fig. 3.

DSSC Anodes	V_{oc} (V)	J_{sc} (mA cm^{-2})	F.F.	η (%)
TiO_2 NR_1	0.71	3.52	0.45	1.11
TiO_2 NR_2	0.68	2.90	0.50	0.99
TiO_2 NR_1–NP	0.71	6.86	0.51	2.51
TiO_2 NR_1–NP–$TiCl_4$	0.72	9.06	0.50	3.25

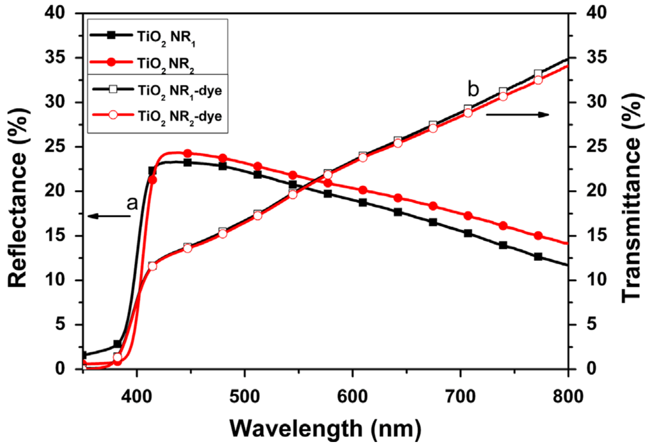

Fig. 4. (a) Diffused reflectance spectra of TiO_2 NR_1 and TiO_2 NR_2 films measured with integrating sphere, the films were illuminated from the TiO_2 side; (b) Transmittance spectra of TiO_2 NR_1 and TiO_2 NR_2 films sensitized by N719 dye, the testing light first contact the glass side into the integrating sphere.

is higher in the visible light wavelength range. This means that the longer TiO_2 nanorods exhibit superior light scattering performance than the shorter ones. However, the transmittance values of both sensitized nanorod anodes with dye are nearly identical from 380 nm to 650 nm, which corresponds to the spectral response range of N719 dye. It suggests that almost similar amount of light was captured by these two different anodes. Therefore, we can conclude that less dye was absorbed on the TiO_2 NR_2 anode due to its smaller internal surface area. As shown in Fig. 1(a), the diameter of TiO_2 NR_2 grows wider and the nanorod roots even form a continuous film. Furthermore, we also notice that the contact between TiO_2 NR_2 and FTO substrate becomes weaker after two step growth that will retard electron collection. As a result, the efficiency of TiO_2 NR_2 cell is lower than that of TiO_2 NR_1 cell, which is contrary to our expectation. Therefore, it proves that this method to improve the cell efficiency by extending TiO_2 nanorod length is infeasible at present.

From Table 1, we can find that TiO_2 NR_1–NP cell has both higher J_{sc} and efficiency of 6.86 mA cm^{-2} and 2.51%, respectively, which is the result of significantly increased surface area of composite anode. The upper TiO_2 film on nanorod arrays composed of P25 nanoparticles increases the anode specific surface area effectively for dye absorption. Simultaneously, the porous structure is beneficial for electrolyte to penetrate through the total TiO_2 composite film. Fig. 3 also compares device performance of TiO_2 NR_1–NP that was treated with or without $TiCl_4$. After surface treatment, J_{sc} increases to 9.06 mA cm^{-2}, and open-circuit voltage (V_{oc}) and filling factor (FF) are both similar to the untreated cell. Consequently, the efficiency reaches to 3.25% with an increment of 29%. The large increase of J_{sc} can be explained as follows. After $TiCl_4$ post-treatment, a thin blocking layer of TiO_2 is deposited on the naked FTO surface that reduces the recombination loss between accumulated electrons and electrolyte [19,20]. Moreover, smaller TiO_2 crystallites grown on the surface of nanorods and nanoparticles composite film will further increase the surface area for more light capture [4]. The different cell photovoltaic conversation behaviors can be further investigated by quantum efficiency measurement.

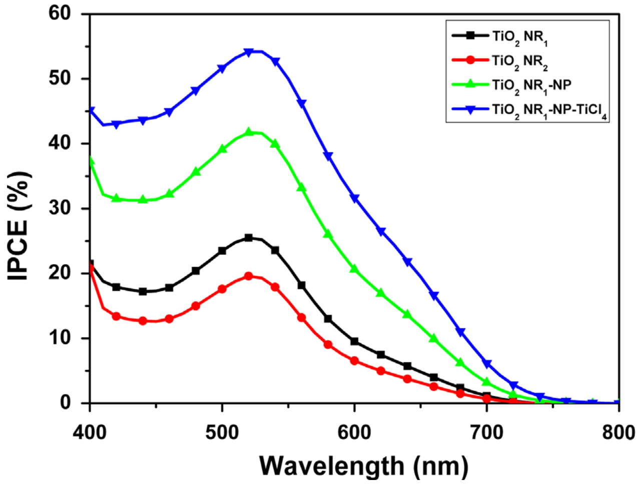

Fig. 5. IPCE spectra of the DSSCs fabricated with TiO_2 NR_1, TiO_2 NR_2, TiO_2 NR_1–NP and TiO_2 NR_1–NP–$TiCl_4$ anodes.

Fig. 5 shows the IPCE spectra of four kinds of DSSCs with different TiO_2 anodes obtained at the short-circuit condition. As can be seen, the IPCE curves from 400 to 700 nm exhibit similar spectrum shape and have an order of TiO_2 $NR_2 <$ TiO_2 $NR_1 <$ TiO_2 NR_1–NP $<$ TiO_2 NR_1–NP–$TiCl_4$ at the visible light wavelength range, which is consistent with J_{sc} order. The IPCE gets a maximum efficiency at 530 nm corresponding to the absorption peak of the N719 dye.

Fig. 6 shows the electrochemical impedance spectra of the above different DSSC devices. Generally, three semicircles can be observed from the impedance spectra in the frequency range of 1–100 mHz, which correspond to the charge transfer resistance at the electrolyte/Pt-electrode interface (R_{pt}), at the TiO_2/dye/electrolyte interface (R_{ct}) and the diffusion resistance of I^-/I^{3-} in the electrolyte (R_{diff}) in succession [21]. As shown in Fig. 6, the first and third semicircles are almost negligible. It means that R_{pt} and R_{diff} are very small in comparison with R_{ct} and indicates that the process of charge transfer at the TiO_2/dye/electrolyte interface is the most dominant factor for the DSSC photovoltaic performance. It is worth mentioning that the minimum value of R_{ct} is observed from TiO_2 NR_1–NP composite DSSC. This indicates that the addition of NP film contributes to the reduction of charge transfer resistance. The R_{ct} is further reduced after $TiCl_4$ treatment that means the conductivity is improved because the nanoparticles connect more closely. As we can see, the R_{ct} value of TiO_2 NR_1 film is the largest close to TiO_2 NR_2 film. This can be attributed to the lowest amount of dye absorption with the result of the lowest electron density injecting to the TiO_2 conduction band. Consequently, the charge transfer process becomes difficult with a result of poor DSSC photovoltaic performance.

Furthermore, the lifetime of electrons (τ) can be estimated from the Bode-phase plots, as shown in Fig. 7, according to the following equation [21]:

$$\tau = \frac{1}{2\pi f_{\min}}$$

where $f_{\min}$ inversely proportional to τ is the minimum frequency of the mid-frequency peak. From Fig. 7, we can find that the electron lifetime of TiO_2 NR_1 film is bigger than that of longer TiO_2 NR_2.

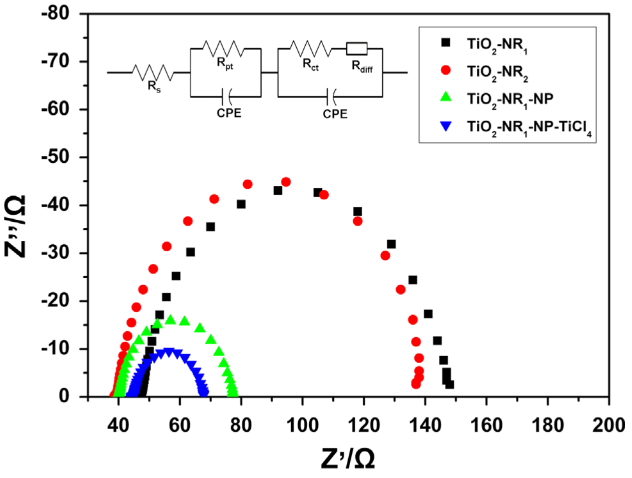

Fig. 6. Nyquist plots of the DSSCs fabricated with TiO_2 NR_1, NR_2, NR_1–NP and NR_1–NP–$TiCl_4$ anodes, respectively, at the open circuit voltage illuminated with AM1.5 solar light of 100 mW cm^{-2}. The inset shows the equivalent circuit for EIS.

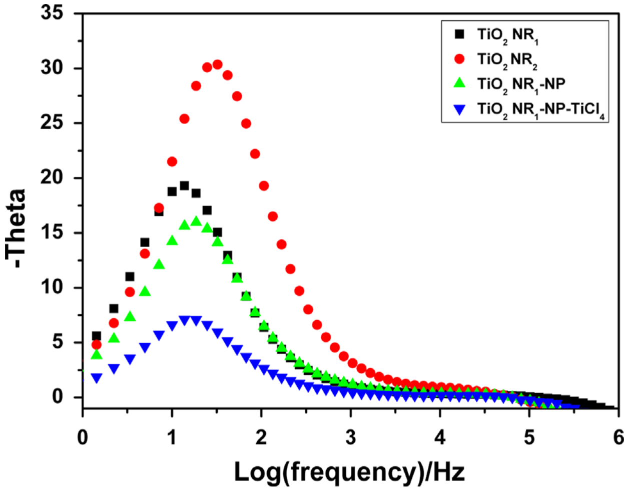

Fig. 7. Bode plots of the DSSCs fabricated with TiO_2 NR_1, NR_2, NR_1–NP and NR_1–NP–$TiCl_4$ anodes, at the open circuit voltage illuminated with AM1.5 solar light of 100 mW cm^{-2}.

Maybe the combination of nanorods at the root as shown in Fig. 1 (a) considerably increases the possibility of electron recombination. However, the frequency peak of TiO_2 NR–NP film moves to left no matter it was treated with $TiCl_4$ or not. This indicates the composite anode has a longer electron lifetime than TiO_2 NR_2 film. At the same time, the electron lifetime of TiO_2 NR_1–NP DSSC only declines slightly in comparison with TiO_2 NR_1 DSSC. This implies that the introduction of NP film can effectively improve the cell photovoltaic conversion efficiency at the expense of slight electron lifetime short.

4. Conclusion

In summary, we first prove that the length increase of TiO_2 nanorods by extending reaction time is infeasible for improving DSSCs efficiency because the longer growth period will lead to combination of nanorods from the roots part and formation of dense film. To overcome this problem, we designed and grew a composite anode consisting of TiO_2 nanorods and mesoporous nanoparticle film. This new type of anode structure combines the advantages of the two parts together. The TiO_2 nanorods offer the direct electron transport pathways with long electron lifetime and enhance light scattering while the mesoporous film supplies large surface area to absorb a large amount of dye. Therefore, a photovoltaic conversion efficiency of 2.51% is obtained from the nanorod–nanoparticle composite film, which is higher than that obtained from pure TiO_2 nanorods DSSC (1.11%). By the another surface treatment process with $TiCl_4$, the DSSC efficiency based on such composite TiO_2 anode is further improved to 3.25%. However, the efficiency is still low, and it has a long way for us to go in order to optimize the composite film.

Acknowledgments

This work is supported by NSFC (51002065 and 11174112) and Shandong Provincial Science Foundation for Disguised Youth Scholars (JQ201214). BC thanks the Taishan Scholar professorship tenured at University of Jinan (TSHW20091007) and the Program for New Century Excellent Talents in University (NCET-11-1027), Ministry of Education, China.

References

[1] B. O'Regan, M. Grätzel, A low-cost, high-efficiency solar cell based on dye-sensitized colloidal TiO_2 films, Nature 353 (1991) 737–740.

[2] D. Wei, Dye sensitized solar cells, International Journal of Molecular Sciences 11 (2010) 1103–1113.

[3] S.H. Han, S. Lee, H. Shin, H.S. Jung, A quasi-inverse opal layer based on highly crystalline TiO_2 nanoparticles: a new light-scattering layer in dye-sensitized solar cells, Advanced Energy Materials 1 (2011) 546–550.

[4] M.S. Wu, C.H. Tsai, T.C. Wei, Electrochemical formation of transparent nanostructured TiO_2 film as an effective bifunctional layer for dye-sensitized solar cells, Chemical Communications 47 (2011) 2871–2873.

[5] A.C. Fisher, L.M. Peter, E.A. Ponomarev, A.B. Walker, K.G.U. Wijayantha, Intensity dependence of the back reaction and transport of electrons in dye-sensitized nanocrystalline TiO_2 solar cells, Journal of Physical Chemistry B 104 (2000) 949–958.

[6] B.V. Zanden, A. Goossens, The nature of electron migration in dye-sensitized nanostructured TiO_2, Journal of Physical Chemistry B. 104 (2000) 7171–7178.

[7] J.V. Lagemaat, A.J. Frank, Nonthermalized electron transport in dye-sensitized nanocrystalline TiO_2 films: transient photocurrent and random-walk modeling studies, Journal of Physical Chemistry B 105 (2001) 11194–11205.

[8] X.J. Feng, K. Shanker, O.K. Varghese, M. Paulose, T.J. Latempa, C.A. Grimes, Vertically aligned single crystal TiO_2 nanowire arrays grown directly on transparent conducting oxide coated glass synthesis details and applications, Nano Letters 8 (2008) 3781–3786.

[9] J.E. Boercker, E. Enache-Pommer, E.S. Aydil, Growth mechanism of titanium dioxide nanowires for dye-sensitized solar cells, Nanotechnology 19 (2008) 095604.

[10] J.Y. Liao, B.X. Lei, Y.F. Wang, J.M. Liu, C.Y. Su, D.B. Kuang, Hydrothermal fabrication of quasi-one-dimensional single-crystalline anatase TiO_2 nanostructures on FTO glass and their applications in dye-sensitized solar cells, Chemistry—A European Journal 17 (2011) 1352–1357.

[11] C.K. Xu, P.H. Shin, L.L. Cao, J. Wu, D. Gao, Ordered TiO_2 nanotube arrays on transparent conductive oxide for dye-sensitized solar cells, Chemistry of Materials 22 (2010) 143–148.

[12] H.P. Wu, L.L. Li, C.C. Chen, E.W.G. Diau, Anodic TiO_2 nanotube arrays for dye-sensitized solar cells characterized by electrochemical impedance spectroscopy, Ceramics International 38 (2012) 6253–6266.

[13] Z.B. Yang, Z.Q. Ma, D.Y. Pan, D.S. Chen, F. Xu, S.M. Chen, Enhancing the performance of front-illuminated dye-sensitized solar cells with highly [001] oriented, single-crystal-like TiO_2 nanotube arrays, Ceramics International (2013) 119, http://dx.doi.org/10.1016/j.ceramint.2013.05.

[14] Z.J. Zhou, J.Q. Fan, X. Wang, W.H. Zhou, Z.L. Du, S.X. Wu, Effect of highly ordered single-crystalline TiO_2 nanowire length on the photovoltaic performance of dye-sensitized solar cells, ACS Applied Materials and Interfaces 3 (2011) 4349–4353.

[15] J. Sheng, L.H. Hu, S.Y. Xu, Characteristics of dye-sensitized solar cells based on the TiO_2/nanoparticle composite electrodes, Journal of Materials Chemistry 21 (2011) 5457–5463.

[16] W.Q. Peng, Y. Masatoshi, L.Y. Han, A. Shahat, Controlled fabrication of TiO_2 rutile nanorod/anatase nanoparticle composite photoanodes for dye-sensitized solar cell application, Nanotechnology 22 (2011) 275709.

[17] B. Liu, E.S. Aydil, Growth of oriented single-crystalline rutile TiO_2 nanorods on transparent conducting substrates for dye-sensitized solar cells, Journal of the American Chemistry Society 131 (2009) 3985–3990.

[18] S. Ito, P. Chen, P. Comte, M.K. Nazeeruddin, P. Liska, P. Pe´chy, M. Grätzel, Fabrication of screen-printing pastes from TiO_2 powders for dye-sensitised solar cells, Progress in Photovoltaics: Research and Applications 15 (2007) 603–612.

[19] A. Burke, S. Ito, H. Snaith, U. Bach, J. Kwiatkowski, M. Grätzel, The function of a TiO_2 compact layer in dye-sensitized solar cells incorporating planar organic dyes, Nano Letters 8 (2008) 971–981.

[20] S.I. Noh, K.N. Bae, H.J. Ahn, T.Y. Seong, Improved efficiency of dye-sensitized solar cells through fluorine-doped TiO_2 blocking layer, Ceramics International 39 (2013) 8097–8101.

[21] R. Kern, R. Sastrawan, J. Ferber, R. Stangl, J. Luther, Modeling and interpretation of electrical impedance spectra of dye solar cells operated under open-circuit conditions, Electrochimica Acta 47 (2002) 4213–4225.